Mechanics of Advanced Composite Structures

Journal homepage: https://macs.semnan.ac.ir/

Semnan University

ISSN: 2423-7043

Research Article

Thermal Behaviour and Coupling Effects in Laminated Composite Beam Structures Using Refined Shear Deformation Theory

Arati Waghmare, Sanjay K. Kulkarni *

Department of Civil Engineering, Symbiosis Institute of Technology, Symbiosis International (Deemed University) Lavale, Pune-412115, Maharashtra, India

ARTICLE INFO

Article history:

Received:
Revised:
Accepted:

Keywords:

Cross-ply;
Quasi 3D theories;
Temperature gradient;
Navier-type series.

ABSTRACT

This study investigates the thermoelastic behaviour of laminated composite beams with symmetric (0/90/0) and asymmetric (0/90) layer-ups subjected to sinusoidally distributed thermal line loads. A quasi-3D shear deformation theory incorporating parabolic and trigonometric through-thickness functions based on Reddy's refined model forms the core analytical framework. The governing equations are derived from the principle of virtual work and solved in closed form via a Navier-type series. The classical beam theory and first-order shear deformation theory are employed solely for comparative analysis. The thermal line load model, representing realistic non-uniform heating scenarios, enables assessments of coupling effects due to laminate asymmetry. Results reveal that asymmetric configurations exhibit significant thermal coupling leading to higher displacements and stress concentrations, while symmetric laminated beams offer improved thermal stability. A MATLAB-based computational tool supports the analysis. The findings underscore the critical role of stacking symmetry in mitigating thermal deformations, guiding the design of reliable composite structures for thermally demanding environments.

1. Introduction

Laminated composite beams have become essential structural elements in modern engineering due to their high strength-to-weight ratio and adaptability in designs. They are widely employed in aerospace, automotive, and civil infrastructure, where components are often exposed to a thermal environment. Accurate modelling of their behaviour is critical as conventional theories may overlook important variations in stress and deformation across the thickness. Advanced analytical approaches are therefore required to ensure the reliable performance of these materials in demanding applications.

The conventional beam theories often fall short in representing the actual variation of stresses and displacements across the thickness, particularly when exposed to non-uniform thermal conditions. A sinusoidal thermal line load generates highly complex stress fields that can not be captured effectively by simplified or lower-order models. To overcome these limitations, it is essential to employ a more

* **Corresponding author.**
E-mail address: sanjay.kulkarni@sitpune.edu.in

Cite this article as:
Mohammadi, A. and Mahdi-Nia, M., 2026. Title of article. *Mechanics of Advanced Composite Structures*, 13(1), pp. xxx-xxx.
https://doi.org/10.22075/MACS.2025.39315.2050

advanced formulation that integrates quasi-3D effects. The present study is directed towards developing and utilizing such a quasi-3D theoretical framework to accurately evaluate the thermal flexural behaviour of laminated beams subjected to sinusoidal thermal line load.

In the hierarchy of equivalent single-layer theories, the Elementary theory of Beam (ETB) or classical beam theory (CBT) stands first. But it can be applied only to thin beams because of its assumption about the nonlinearity of the mid-surface plane. This theory was applied by Chen et al. [1] to assess the effect of thermal loading on laminated beams. Furthermore, Timoshenko [2] developed a theory for beams taking into account first-order shear effects and rotational inertia within the kinematic framework of the theory. This model, called the Timoshenko theory of beams, represents a first-order shear theory. It considers shear deformation effects by including a constant shear correction factor. Miglani J. et al. [3] adopted the first-order deformation theory for analysing periodically supported laminated beams. A sensitivity analysis was done that gave knowledge about the location of supports. Chen et al. [4] compared the results of classical theory and Timoshenko beam theory to analyze symmetrical cross-ply laminated composite beams. Kapuria et al. [5] applied first-order shear deformation and classical lamination theories to Piezoelectric plates subjected to thermoelectromechanical load. In both above-mentioned theories (ETB and FSDT), the transverse shear strain was considered as constant in the thickness direction. Also, the factors introduced in the first-order theory were difficult to determine for anisotropic composite structures. Hence, higher-order theories were developed that removed the inextensibility condition and perpendicular straightness of the transverse normal. Researchers used different displacement fields and obtained results as stresses and displacements.

Touratier [6] obtained the stresses and displacements for a laminated and sandwich plate by introducing a sinusoidal function in the displacement field. A refined displacement-based theory for the analysis of symmetric laminated plates subjected to both thermaland mechanical loads was presented by Ali et al. [7]. The author provided a unified framework that is computationally efficient and closely aligned with three-dimensional elasticity solutions, making it a strong alternative to rigorous full 3D analysis. Adopting the equivalent single-layer theory, the displacement model was presented by Robaldo and Carrera [8], considering Murakami's concept in the zigzag form.

T. Kant and A. Gupta [9] incorporated a quadratic spread of transverse shearing strain and transverse normal strain in a linear way through the thickness of the beam. It was concluded that for beams with a lower side-to-thickness ratio, displacements computed by using thin beam theory are smaller than the true values, and natural frequencies are higher than the true values as transverse shear energy is neglected. Khedir and Reddy [10] analyzed cross-ply rectangular beams with various support conditions and presented a comparison between the results of different shear deformation theories. Considering the effect of transverse normal deformation, Sarath and Kant [11] had employed two refined higher-order theories. Ghugal and Shimpi [12] reviewed various articles based on refined theories adopted for isotropic and anisotropic laminated beams and compared the results with each other.

Arya et al. [13] presented a zigzag model for the beam, adopting trigonometric terms to represent the nonlinear displacement field and strain along the thickness direction. E. Carrera [14] quoted the very important conclusion that in layered structures, transverse normal strain plays a crucial role affecting the behavior of stresses. Further, Carrera et al. [15] compared different approaches applied to beams. Aydogdu [16] analyzed cross-ply laminated beams subjected to thermal buckling using a shear deformable beam theory with three degrees of freedom at every node and the minimum energy principle. The Ritz method is used for obtaining critical thermal temperatures. A hyperbolic higher-order theory was developed by Ghugal and Sharma [17] to obtain flexural vibrations and static flexural response of thick isotropic beams. A thermo-mechanical finite element formulation for laminated beams, accounting for both mechanical and thermal effects, was presented by Vidal and Polit [18]. Sayyad [19] applied the unified refined theory by following the unknowns from first-order shear deformation theory and obtained the shear deformation, stresses, and natural frequencies for the thick isotropic beam. Sayyad and Ghugal [20] presented the analysis of beams subjected to a variety of mechanical loads. Symmetrical angle-ply shear deformation laminated composite beam subjected to transversely uniform temperature was analyzed by Chang et al. [21]. Ghugal and Dahake [22] adopted a sinusoidal function to represent the displacement field in the thickness direction and developed a theory for the flexural analysis of a thick fixed beam.

Assuming every layer of the beam as linearly elastic and fiber-reinforced, shear deformable

anisotropic laminated beams facing constant temperature across the thickness were analyzed by Li Z. M. and Qiao P. [23] for different boundary conditions. Buckling temperatures were obtained using Galerkin's method. Mohammadabadi et al.[24] analyzed micro composite laminated beams by applying the couple stress modified theory and adopted the generalized differential quadrature (GDQ) method for obtaining governing equations in the analysis of cross ply laminated beams. Based on equivalent theories, exact theories, layerwise theories, and zigzag theories, Sayyad and Ghugal [25] presented a critical review of the literature. The authors summarized displacement fields of various theories, which can be of extreme help for future research. The analytical thermoelastic solutions for layered composite plates with orthotropic and fully anisotropic material behaviour were presented by Bhaskar et al. [26]. Their work focused on predicting temperature-induced stresses and deformations by using an exact elasticity-based formulationrather than simplified plate theories. Vidal and Polit [27] introduced an enhanced finite element formulation for laminated beams that incorporates a sine-based displacement field along with transverse normal deformation. Kenanda et al. [28] developed a new shear deformation theory based on logarithmic-hyperbolic shape function to study how porous functionally graded materials behave under thermal and mechanical loads. Taibi et al. [29] investigated how different micromechanical models used to predict thermal expansion affect the behaviour of laminated composite plates under temperature variations. Kenanda et al. [30] developed an advanced plate model that can more accurately describe how porous functionally graded plates and nanoplates vibrate. Their formulation combines a hyperbolic higher-order shear deformation theory with nonlocal elasticity so that both thickness-wise deformationand small-scale effects are captured. Reddy [31] formulated a higher-order shear deformation theory by adapting a displacement field with a cubic variation through the laminate thickness, which naturally drives the transverse shear stresses to zero on the outer surfaces. Localized stress behaviour in engineering components has been extensively investigated by Radojkovic et al. [32], and studies show that square-shaped openings act as significant points of stress intensification within machine elements. Artificial intelligence and machine learning techniques have been increasingly applied to engineering problems, including predictive maintenance and lifecycle optimization of electric vehicles, as presented by Marinkovic et al. [33]. Recently, the work based on optimizing the tribological performance of aluminium-based composites using a combination of Taguchi method, Grey Relational Analysis (GRA), and TOPSIS was presented by Gajevic et al. [34]. The authors demonstrate how these statistical tools can be used to identify optimal material compositionsand processing parameters that minimize wear and friction, contributing to cost-effective material performance.

Despite extensive research on the thermal behaviour of laminated composite structures, most existing studies focus on mechanical loadings. While the higher-order theories have gained traction, comparative assessments between antisymmetric and symmetric laminates under thermal line load remain limited. Moreover, the coupling phenomenon where thermal loads induce unintended mechanical responses due to laminate asymmetry has not been thoroughly quantified using refined shear deformation models such as trigonometric (TSDT) and parabolic (PSDT) formulations. The lack of analytical clarity regarding how laminate symmetry influences thermal displacement and stress distribution presents a critical gap. This study also addresses the application of advanced shear deformation theories to model thermal effects precisely, comparing symmetric and asymmetric configurations under identical thermal conditions and demonstrating the pronounced coupling in antisymmetric laminates, the thermal resilience of symmetric ones. Such insights are essential for engineers designing thermally loaded composite structures, where laminate architecture directly impacts performance and reliability.

2. Methodology

In many engineering fields like aerospace, electronics, and automotive engineering, composite laminated beams are often exposed to uneven heating. This happens due to focused heat sources such as lasers, solar energy, or internal electronic components, which create thermal line load along the beam. The welding along a line can also be considered as a sinusoidal thermal line load for analytical modelling. The laminated beams can be stacked in various layer configurations, and the symmetry of the stacking sequence plays a crucial role in how the beam structure responds to thermal loads. Hence, Symmetric and antisymmetric laminated composite beams are studied to understand how layer configuration or stacking sequence affects thermal deformations and stress behaviour under such heating.

Two cross-ply laminated beams, antisymmetric (0/90) and symmetric (0/90/0), are considered for analysis. Length of beam is L, and it has a thickness h ranging from $\left(-\frac{h}{2}\right)$ (at top) to $\left(+\frac{h}{2}\right)$ (at bottom). The sinusoidal thermal line load is applied at the top of the beam ($z = -\frac{h}{2}$). The configuration of the two-layer and three-layer beam is shown in Figure 1. The x and z axes are labeled to indicate in-plane and through-thickness directions, respectively.

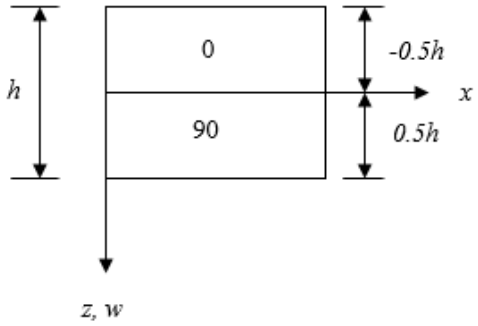

(a)

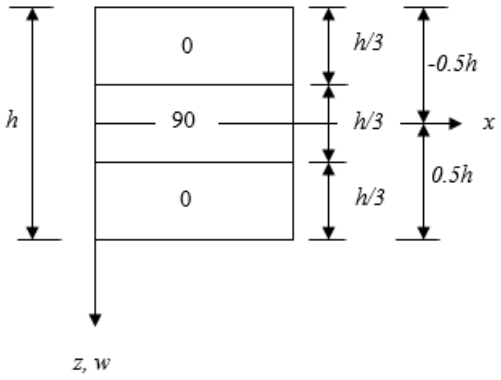

(b)

Fig. 1. The configuration of two-layer and three-layer beams

The trigonometric and parabolic shear deformation models have unique mathematical expressions to capture shear strain variation through the thickness of the laminated beam. The assumptions of these theories are as follows.

1. The beam is simply supported.
2. The beam consists of orthotropic layers
3. The effect of transverse normal is added to the theory.
4. The displacements in the y direction are neglected due to the small width b in this direction.
5. The sinusoidal thermal line load is taken into consideration during analysis.

In structural mechanics, trigonometric shear deformation theory (TSDT) is a well-advanced approach used to study the bending response of laminated beams under loads. This theory includes a sinusoidal function in the displacement field, which represents a shear effect in a better way. The displacement field of this theory is as follows.

$$(x,z) = u_0 - z\frac{\partial w}{\partial x} + \frac{h}{\pi} sin\frac{\pi z}{h}\varphi(x) \quad (1)$$

$$w = w_0 + cos\frac{\pi z}{h}\xi(x) \quad (2)$$

Another higher-order approach frequently applied in structural mechanics for evaluating the thermal bending of laminated beams is the parabolic theory (PSDT). In this case, the transverse shear stress is assumed to vary parabolically through the beam thickness. The displacement field expressions for this theory are written as:

$$u\,(x,z) = u_0 - z\frac{\partial w}{\partial x} + z\left(1 - \frac{4z^2}{3h^2}\right)\varphi(x) \quad (3)$$

$$w(x,z) = w_0 + \left(1 - \frac{4z^2}{h^2}\right)\xi(x) \quad (4)$$

In the above equations (3) and (4), $u\,(x,z)$ and w(x, z) are displacements in the x and z directions respectively. The mid-plane displacement is represented by u_0 at $(z = 0)$. The function $\varphi(x)$ and $\xi(x)$ are the unknown rotations.

2.1. Strain Components

Normal strains ε_x, ε_z and transverse shear strains γ_{zx} are derived from the equations of displacement fields. These strain-displacement relations, as given below, are necessary for accurate modelling.

$$\varepsilon_x = \frac{\partial u}{\partial x} = \frac{\partial u_0}{\partial x} - z\frac{\partial^2 w}{\partial x^2} + z\left(1 - \frac{4z^2}{3h^2}\right)\frac{\partial \varphi}{\partial x} \quad (5)$$

$$\varepsilon_z = \frac{\partial w}{\partial z} = -\left(\frac{8z}{h^2}\right)\xi \quad (6)$$

$$\gamma_{zx} = \frac{\partial u}{\partial z} + \frac{\partial w}{\partial x} = \left(1 - \frac{4z^2}{h^2}\right)\left(\varphi + \frac{\partial \xi}{\partial x}\right) \quad (7)$$

The equation (5) represents normal strain in x direction ε_x incorporates mid-plane strain, bending curvature, and higher-order terms which involve rotation ∅. The equation (6) gives the normal strain in the z direction i.e ε_z, which is related to the thickness coordinate z and the warping function ξ. Equation (7) describes the shear strain γ_{zx} capturing both transverse shear deformation and its variation through the thickness. These relations are crucial for accurately modelling the behaviour of thick laminated beams.

2.2. Constitutive Relations

The constitutive relations are derived from generalized Hook's law for anisotropic materials tailored for thermoelastic behaviour of composite laminated beams, represented by equations (8) and (9) in local and global coordinate systems as below.

2.2.1 Local Coordinate System

In the local coordinate system, aligned with principle directions i.e. fibre direction 1, and transverse direction 3, the constitutive relation is as below.

$$\begin{bmatrix}\sigma_1\\ \sigma_3\\ \sigma_{13}\end{bmatrix}=\begin{bmatrix}Q_{11} & Q_{13} & 0\\ Q_{13} & Q_{33} & 0\\ 0 & 0 & Q_{55}\end{bmatrix}\begin{Bmatrix}\varepsilon_1-\alpha_1 T\\ \varepsilon_3-\alpha_3 T\\ \gamma_{13}-\alpha_{13}T\end{Bmatrix} \quad (8)$$

where, Q_{ij} are reduced stiffness coefficients in the lamina coordinate system. The coefficient of thermal expansion in local direction is represented by α_i. The temperature change is denoted by T in the above equation.
To analyze the laminated beam, the local stiffness matrix is transformed to the global coordinate system using standard transformation relations.

2.2.2 Transformation Relations:

To find $\bar{Q}_{ij}$ from Q_{ij} the following transformation equations for a rotation angle θ, measured anticlockwise from the global axis x to the local axis-1.

$$\bar{Q}_{11}=Q_{11}cos^4\theta+2Q_{13}cos^2\theta sin^2\theta+Q_{33}sin^4\theta \quad (8a)$$

$$\bar{Q}_{33}=Q_{11}sin^4\theta+2Q_{13}cos^2\theta sin^2\theta+Q_{33}cos^4\theta \quad (8b)$$

$$\bar{Q}_{13}=(Q_{11}+Q_{33}-2Q_{13})cos^2\theta sin^2\theta+Q_{13}(cos^4\theta+sin^4\theta) \quad (8c)$$

$$\bar{Q}_{55}=(Q_{55})\,(cos^2\theta-sin^2\theta)^2 \quad (8d)$$

2.2.3 Angle and Sign Convention:

The angle between the global x axis and the local axis 1 i.e fibre direction is denoted by θ. This angle θ is treated as positive when measured in counterclockwise rotation from x axis to fibre axis 1. The stress and strain components follows standard tensor transformation rules. By using these standard transformation rules the global coordinate system can be obtained as below.

2.2.4 Global Coordination System:

The constitutive relation in global coordinate system (x-z-xz) is as below.

$$\begin{bmatrix}\sigma_x\\ \sigma_z\\ \sigma_{zx}\end{bmatrix}=\begin{bmatrix}\bar{Q}_{11} & \bar{Q}_{13} & 0\\ \bar{Q}_{13} & \bar{Q}_{33} & 0\\ 0 & 0 & \bar{Q}_{55}\end{bmatrix}\begin{Bmatrix}\varepsilon_x-\alpha_x T\\ \varepsilon_z-\alpha_z T\\ \gamma_{xz}-\alpha_{xz}T\end{Bmatrix} \quad (9)$$

This equation models how thermal expansion affects the stress state in a composite laminated beam. In above equations $\bar{Q}_{ij}^{(k)}$ is the reduced stiffness coefficient in x-z plane. Thermal strain due to temperature change T in *the* x and z directions is represented by $\alpha_x T$ and $\alpha_z T$ respectively. The above equation shows that the normal stress σ_x in x direction is influenced not only by strain in x but also by strain and thermal expansion in the z direction due to material anisotropy. The normal stress in the z direction and shear stress in the x-z plane are denoted by σ_z and σ_{zx} respectively. When temperature changes, the material expands, and this behaviour is anisotropic, i.e., directional dependent in composite laminated beams. The above accounts for mechanical deformation via strain terms, thermal effects via αT terms and material anisotropy via $\bar{Q}_{ij}^{(k)}$. In cross-ply laminated beams, each ply is aligned either along or perpendicular to the principal axis, eliminating angular transformation effects and preserving direct stiffness terms. This alignment ensures that the global stiffness coefficients match the local ones for 0^0 and 90^0 orientations. Hence, the relationship between stiffness coefficients and elastic constants is given by:

$$\bar{Q}_{11}^{(k)} = \frac{\bar{E}_1^{(k)}}{\left(1-\mu_{13}^{(k)}\mu_{31}^{(k)}\right)} \tag{10}$$

$$\bar{Q}_{13}^{(k)} = \frac{\mu_{13}^{(k)}\bar{E}_1^{(k)}}{\left(1-\mu_{13}^{(k)}\mu_{31}^{(k)}\right)} \tag{11}$$

$$\bar{Q}_{33}^{(k)} = \frac{\bar{E}_3^{(k)}}{\left(1-\mu_{13}^{(k)}\mu_{31}^{(k)}\right)} \tag{12}$$

$$\bar{Q}_{55}^{(k)} = \bar{G}_{13}^{(k)} \tag{13}$$

In the above equations E_1 and E_3 denotes the Young's modulus, G_{55} represents shear modulus and μ_{13}, μ_{31} indicates Poisson's ratios. The subscripts 1 and 3 represent directions along *x* and *z*, respectively.

2.3. Thermal Profile

The temperature field represented by the following equation (14) represents a sinusoidal thermal line load when *m* = 1.

$$T(x,z) = \left[T_0(x) + \left(\frac{2z}{h}T_1\right) sin\left(\frac{m\pi x}{a}\right)\right] \tag{14}$$

In the above equation (14), the term $sin\left(\frac{m\pi x}{a}\right)$ introduces a periodic thermal profile, which is the characteristic of a thermal line load. This is a localized heating effect that varies smoothly along the beam. The factor $\frac{2z}{h}$ ensures that the temperature changes linearly from the top to the bottom surface, as in thermal bending problems. The term T_1 represents the amplitude which controls the intensity of the thermal gradient. The base temperature is represented by (T_0) and is constant. For m =1, the sine function completes one half wave over the beam length *a,* which models a single localized heating zone ideal for simulating a thermal line load. The Fourier coefficient $T_{om} = \frac{2T}{a} sin\frac{m\pi}{2}$ ensures that the thermal inputs are mathematically consistent with a sinusoidal distribution. The above equation of temperature field models a sinusoidal thermal line load, which is a realistic representation of localized heating in composite laminated beams.

2.4. Motion Governing Equations and Support Conditions

In structural mechanics, the virtual work principle is a fundamental concept to analyse the deformations in the laminated beam structures. The principle of virtual work has previously been applied in the development of governing equations by Reddy [31]. Building on this established approach, the present study introduces a quasi-3D framework designed to capture the thermal flexural response of laminated beams subjected to sinusoidal thermal line loading.

This principle states that total virtual work done by internal stresses and external forces must be zero for equilibrium and is represented by equation (15) as given below.

$$\int_{z=-\frac{h}{2}}^{z=+\frac{h}{2}} \int_{x=0}^{x=a} (\sigma_x \delta\varepsilon_x + \sigma_z \delta\varepsilon_z + \tau_{zx}\delta\gamma_{zx})dxdz - \int_0^a q\,\delta w\,dx = 0 \tag{15}$$

The governing equations are solved by using integration by parts. By collecting successive terms of δu_0, δw, $\delta\varphi$ and $\delta\xi$ and equating them to zero, the following governing equations are obtained.

$$\delta u_0 : -A_{11}\frac{\partial^2 u_0}{\partial x^2} + B_{11}\frac{\partial^3 w}{\partial x^3} - \left(B_{11} - \frac{4}{3h^2}E_{11}\right)\frac{\partial^2\varphi}{\partial x^2} + \frac{8}{h^2}B_{13}\frac{\partial\xi}{\partial x} + (TA_{11} + TA_{13})\frac{\partial T_0}{\partial x} + \frac{2}{h}(TB_{11} + TB_{13})\frac{\partial T_1}{\partial x} = 0 \tag{16}$$

$$\delta w: -B_{11}\frac{\partial^3 u_0}{\partial x^3}+D_{11}\frac{\partial^4 w}{\partial x^4}-\left(D_{11}-\frac{4}{3h^2}F_{11}\right)\frac{\partial^3 \varphi}{\partial x^3}+(TB_{11}+TB_{13})\frac{\partial^2 T_0}{\partial x^2}+\frac{2}{h}(TD_{11}+TD_{13})\frac{\partial^2 T_1}{\partial x^2}+\frac{8}{h^2}D_{13}\frac{\partial^2 \xi}{\partial x^2}=0 \quad (17)$$

$$\delta\varphi: -\left(B_{11}-\frac{4}{3h^2}E_{11}\right)\frac{\partial^2 u_0}{\partial x^2}+\left(D_{11}-\frac{4}{3h^2}F_{11}\right)\frac{\partial^3 w}{\partial x^3}-\left(D_{11}+\frac{16}{9h^4}H_{11}-\frac{8}{3h^2}F_{11}\right)\frac{\partial^2 \varphi}{\partial x^2}+\left(TB_{11}-\frac{4}{3h^2}TE_{11}\right)\frac{\partial T_0}{\partial x}+\left(TD_{11}-\frac{4}{3h^2}TF_{11}\right)\frac{2}{h}\frac{\partial T_1}{\partial x}+\left(TB_{13}-\frac{4}{3h^2}TE_{13}\right)\frac{\partial T_0}{\partial x}+\left(TD_{13}-\frac{4}{3h^2}TF_{13}\right)\frac{2}{h}\frac{\partial T_1}{\partial x}+\left(A_{55}-\frac{4}{h^2}D_{55}\right)\varphi+\left(-\frac{4}{h^2}D_{55}+\frac{16}{h^4}F_{55}\right)\varphi+\left(\frac{8}{h^2}D_{13}-\frac{32}{3h^2}F_{13}\right)\frac{\partial \xi}{\partial x}=0 \quad (18)$$

$$\delta\xi: -\frac{8}{h^2}B_{13}\frac{\partial u_0}{\partial x}+\frac{8}{h^2}D_{13}\frac{\partial^2 w}{\partial x^2}-\left(\frac{8}{h^2}D_{13}-\frac{32}{3h^2}F_{13}\right)\frac{\partial \varphi}{\partial x}+\frac{8}{h^2}TB_{12}T_0+\frac{16}{h^3}TD_{12}T_1+\frac{64}{h^4}D_{33}\xi+\frac{8}{h^2}TB_{33}T_0+\frac{16}{h^3}TD_{33}T_1-\left(A_{55}-\frac{8}{h^2}D_{55}+\frac{16}{h^4}F_{55}\right)\frac{\partial \varphi}{\partial x}-\left(A_{55}-\frac{8}{h^2}D_{55}+\frac{16}{h^4}F_{55}\right)\frac{\partial^2 \xi}{\partial x^2}=0 \quad (19)$$

The terms in the governing equations are verified to maintain dimensional homogeneity. The primary variables $u_0, w, \emptyset$ and ξ represents displacements and rotations, and their derivatives are checked against the units of corresponding coefficients. Table 1, below summarize the physical units of all coefficients and variables used in the governing equations.

Table 1. Physical units of coefficients and variables

Symbol	Description	Unit
A_{11}	Axial Stiffness	N/m
B_{11}	Bending Stiffness	N-m
D_{11}	Flexural rigidity	N-m^2
E_{11}	Thermoelastic coupling coefficient	N
F_{11}	Higher-order thermoelastic term	N-m
H_{11}	Thermal moment coefficient	N-m^2
T_0, T_1	Temperature fields	K
u_0, w	Displacements	meter
$\emptyset, \xi$	Rotations	radian
h	Thickness of the beam	Meter

Each term has a unit of force per unit length (N/m) to be consistent. Some derivatives are examined below.

$A_{11}\frac{\partial^2 u_0}{\partial x^2} = (N/m) \times (1/m) = N/m^2$

In structural mechanics A_{11} represents axial stiffness per unit width, and it has the unit of A_{11}= Force/Length=N/m. Then the further term $\frac{\partial^2 u_0}{\partial x^2}$. The term $\frac{\partial^2 u_0}{\partial x^2}$ has units of displacement per length square, i.e. m^{-1}. Hence, the product becomes (N/m). (1/m) = N/m^2.

Normalization Procedure:

To make the equations easier to work with and suitable for numerical analysis, a basic scaling method is used, known as normalization. This helps to reduce the complexity of the terms and ensure consistency across different units. The rotation $\emptyset$ is assumed to be dimensionless unless otherwise stated. The shear deformation variable ξ is normalized by plate thickness h. The temperature fields T_0, T_1 are normalized by reference temperature. All displacement values are divided by a chosen reference displacement u_{ref}. The material constants are kept in their original units but are used in combination with the scaled variables to maintain correct dimensions. The normalized variables are written with a bar on top, for example $\bar{u}_0 = \frac{u_0}{u_{ref}}$. This approach helps to simplify the mathematical expressions and ensure that all terms are dimensionally consistent.

The boundary constraints at $x = 0$ and $x = a$ are as given below.

$$N_x = A_{11}\frac{\partial u_0}{\partial x} - B_{11}\frac{\partial^2 w}{\partial x^2} + \left(B_{11} - \frac{4}{3h^2}E_{11}\right)\frac{\partial \varphi}{\partial x} - \frac{2}{h}(TB_{11} + TB_{13})\,T_1 - (TA_{11} + TA_{13})\,T_0 = 0 \text{ or } u_0 \text{ is prescribed} \tag{20}$$

$$V_x = B_{11}\frac{\partial^2 u_0}{\partial x^2} - D_{11}\frac{\partial^3 w}{\partial x^3} + \left(\mathrm{D}_{11} - \frac{4}{3h^2}\mathrm{F}_{11}\right)\frac{\partial^2 \varphi}{\partial x^2} - (TB_{11} + TB_{13})\frac{\partial T_0}{\partial x} - \frac{2}{h}(TD_{11} + TD_{13})\frac{\partial T_1}{\partial x} - \frac{8}{h^2}D_{13}\frac{\partial \xi}{\partial x} = 0 \text{ or } w_0 \text{ is prescribed} \tag{21}$$

$$M_x^s = \left(B_{11} - \frac{4}{3h^2}E_{11}\right)\frac{\partial u_0}{\partial x} - \left(D_{11} - \frac{4}{3h^2}F_{11}\right)\frac{\partial^2 w}{\partial x^2} + \left(D_{11} + \frac{16}{9h^4}H_{11} - \frac{8}{3h^2}F_{11}\right)\frac{\partial \varphi}{\partial x} - \left(\frac{8}{h^2}D_{13} - \frac{32}{3h^2}F_{13}\right)\xi - \left(TB_{11} - \frac{4}{3h^2}TE_{11}\right)T_0 - \left(TD_{11} - \frac{4}{3h^2}TF_{11}\right)\frac{2}{h}T_1 - \left(TB_{13} - \frac{4}{3h^2}TE_{13}\right)T_0 - \left(TD_{13} - \frac{4}{3h^2}TF_{13}\right)\frac{2}{h}T_1 = 0 \text{ or } \varphi \text{ is prescribed} \tag{22}$$

$$M_x^b = -\left(D_{11} - \frac{4}{3h^2}F_{11}\right)\frac{\partial \varphi}{\partial x} + + \frac{8}{h^2}D_{13}\,\xi + (TB_{11} + TB_{13})T_0 + \frac{2}{h}(TD_{11} + TD_{13})\,T_1 = 0 \text{ or } \frac{\partial w}{\partial x} \text{ is prescribed} \tag{23}$$

Physical interpretation of boundary conditions:

The boundary conditions presented in equations (20) –(23) correspond to the generalized stress resultants acting at the beam edges $x = 0$ and $x = a$. Each equation expresses the equilibrium between mechanical and thermal effects for different deformation variables. Their physical meanings are clarified below.

1. Axial boundary condition (Equation 20):

This condition represents the axial force equilibrium along the beam edge. The term N_x denotes the in-plane normal force per unit width acting in the x direction. The expression involves contributions from the mid-plane normal strain $\left(\frac{\partial u_0}{\partial x}\right)$, the bending curvature $\left(\frac{\partial^2 w}{\partial x^2}\right)$ and the higher-order rotation gradient $\left(\frac{\partial \emptyset}{\partial x}\right)$ together with thermal-induced forces arising from temperature fields T_0 and T_1. Physically, this boundary is either traction-free when $N_x = 0$ or kinematically prescribed when the in-plane displacement u_0 is specified.

2. Transverse shear boundary condition (Equation 21):

The second condition defines the transverse shear force resultant V_x which ensures equilibrium of the out-of-plane shear at the edge. The various terms account for coupling between stretching, bending, and shear deformationsas well as temperature gradients through T_0, T_1 and ξ.

When $V_x = 0$, the edge is free of transverse shear while prescribing w_0 corresponds to a simply supported edge depending on the other constraints.

3. Surface moment boundary condition (Equation 22):

The equation (22) corresponds to the shear moment resistance M_x^s associated with the rotation variable ∅. This moment combines bending and shear effects in higher-order theories and includes contributions from the thermal moments generated by through-thickness temperature variation. A condition M_x^s represents a free rotation at the surface, while specifying ∅ implies a rotationally constrained boundary.

4. Bending Moment boundary condition (Equation 23):

Equation (23) defines the bending moment resultant M_x^b, primarily linked with the curvature $\left(\frac{\partial^2 w}{\partial x^2}\right)$. It balances the bending deformation, higher-order shear interaction, and thermal bending moments. A zero value of M_x^b implies a moment free i. e., simply supported edge, whereas prescribing the slope $\left(\frac{\partial w}{\partial x}\right)$ represents a clamped edge.

The equations (20)-(23) collectively specify the thermal boundary behaviour of the laminated beam.

In the above equations, stiffness coefficients for the lamina are given by

$$\left(A_{ij}, B_{ij}, D_{ij}, E_{ij}, F_{ij}, H_{ij}\right) = \sum_{k=1}^{N} \int_{z=k}^{k+1} \bar{Q}_{ij}^{(k)} \left(1, z, z^2, z^3, z^4, z^6\right) dz \quad (24)$$

$$TA_{ij}, TB_{ij}, TD_{ij}, TE_{ij}, TF_{ij} = \sum_{k=1}^{N} (\alpha_x) \int_{z=k}^{k+1} \bar{Q}_{ij}^{(k)} \left(1, z, z^2, z^3, z^4\right) dz \quad (25)$$

The coefficients $\left(A_{ij}, B_{ij}, D_{ij}, E_{ij}, F_{ij}, H_{ij}\right)$ represents generalized stiffness matrices of the laminated beam and describe how inplane, bending and higher-order deformation modes are coupled through the thickness.

A_{ij} : Extensional stiffness relating inplane forces to mid-plane strains.

B_{ij} : Bending-streching coupling stiffness. This represents coupling between inplane deformationand bending curvature.

D_{ij} : Corresponds to bending stiffness, which relates applied bending moments to resulting curvature.

E_{ij}, F_{ij}, H_{ij}: Captures higher-order stiffness effects, accounting for the influence of transverse shear deformation and nonlinear through-thickness strain variations, which become significant in refined beam theories.

For a laminate that is symmetric about the mid-plane, the coupling matrix B_{ij} and thermal coupling term TB_{ij} vanishes. As a result, bending and in-plane deformations occur independently and no coupling exists between the two. However, in an asymmetric laminate configuration the B_{ij} and other higher-order coupling coefficients remain nonzero. In such cases, stretching may induce bending moment and these bending moments can generate in-plane deformations. This is an important characteristic that influences the global response of structure. The thermal coefficients $TA_{ij}, TB_{ij}, TD_{ij}, TE_{ij}, TF_{ij}$ in equation (25) describe the thermal stiffness ontributions, representing in-plane forces and moments generated due to temperature gradientsacross the laminated beam thickness.

2.4.1 Closed Form Solution

The analytical solution is derived through Navier's approach, ensuring that the boundary conditions are precisely satisfied along the edges positioned at *x = 0* and *x = a.*

$$w = 0, M_x = 0, N_x = 0, M_x^s = 0$$

The condition $w = 0$ indicates that the vertical or transverse displacement of the beam at the boundary is constrained due to a simply supported edge that prevents movement in the z direction. The bending moment in the x direction is zero, i. e. $M_x = 0$ indicates that there is no resistance to bending at the edge in x direction. Since the edge is simply supported, the edge is free to rotate without any moment applied. The axial force in x direction is zero i. e. $N_x = 0$, implies that no in-plane force acts along the x direction at the boundary. This means that the edge is not subjected to tension or compression. The shear moment M_x^s is zero. This represents the higher-order moment due to transverse shear deformation. This condition ensures a realistic shear stress distribution and satisfies natural boundary conditions.

The following unknowns are represented in trigonometric form, which satisfy the exact boundary conditions. The expansion of thermal loads is in the form of a single Fourier sine series, as shown below.

$$u_0, \varphi_0 = \sum_{m=1}^{\infty} \left(u_m, \varphi_m \cos\frac{m\pi x}{a}\right) \quad (26)$$

$$w_0, \xi_0 = \sum_{m=1}^{\infty} \left(w_m, \xi_m \sin\frac{m\pi x}{a}\right) \quad (27)$$

$$T_0, T_1 = \sum_{m=1}^{\infty} \left(T_{0m}, T_{1m} \sin\frac{m\pi x}{a}\right) \quad (28)$$

The thermal line load is acting parallel to the length "L" of the beam and placed centrally. The Fourier sine coefficient (28) is the standard sine-series formula. Then the term $T_{0m} = \frac{2}{a}\int_0^a T_0(x) sin\frac{m\pi x}{a} dx$ is the next step. Further, the thermal line load is at the mid-span $x = \frac{a}{2}$ with total magnitude T, the integral gives the closed form $T_{om} = \frac{2T}{a} sin\frac{m\pi}{2}$. For even m, $sin\frac{m\pi}{2} = 0$, and alternates ± 1 for odd m. Therefore, odd harmonics appear.

In the above equations from (26) to (28) $u_m, \varphi_m, w_m, \xi_m, T_{0m}, T_{1m}$ are unknowns to be determined. Once these unknown coefficients are evaluated, one can substitute them into governing equations (16) -(19) to get thermal deformations.

2.4.2 Numerical Implementation:

After formulating the governing equations, a MATLAB program is developed to calculate the thermal deformation behaviour of the laminated composite beam. The purpose of this implementation is not to introduce a new computational scheme, but to provide a practical tool for solving the higher-order coupled equations under thermal loading. The program evaluates the stiffness matrices, applies the required discretization for the differential equations, and incorporates the boundary condition given in equations (20) – (23).

The computational analysis was conducted using the specified hardware, Processor Intel® Core ™ i7-6820HQ CPU@2.70 GHz, set up. The numerical modelling was performed through MATLAB, 7.5.0 R2007b, provided by MathWorks.

2.5. Computation of Transverse Shear Stress

To maintain continuity of the inter-laminar shear stresses at the interfaces, the equation of equilibrium is utilized to evaluate the shear stresses. Transverse shear stress computed by using the equilibrium equation is denoted by τ_{zx}^{EE}. The equation to evaluate the transverse shear stress is as given below.

$$\tau_{zx}^{EE} = -\int_{z=-h/2}^{+h/2} \frac{\partial \sigma_x}{\partial x}\, dz + C \qquad (29)$$

The term τ_{zx}^{EE} is transverse shear stress in *z-x* plane evaluated from the equilibrium equation. The normal stress σ_x in the *x* direction varies through the thickness. The term $\frac{\partial \sigma_x}{\partial x}$ is the spatial rate of change of axial stress along the *x* direction. The thickness coordinate *z* ranges from *-h/2* to *h/2* i. e., from top to bottom of the beam, where *h* is the total thickness of the beam. The integration constant *C* is determined by enforcing appropriate boundary constraints. The resulting transverse shear stress conforms to the requirement of a stress-free surface at both the upper and lower faces of the beam. This equation (29) captures realistic shear behaviour across the thickness of the beam.

2.6. Material Characteristics

The mechanical characteristics utilized in this study are sourced from the work of Bhaskar et al. [26]. In the context of fibre orientation, the terms *L* and *T* are used to denote the longitudinal and transverse axes, respectively.

$$\frac{E_T}{E_L} = 25;\ \frac{\alpha_T}{\alpha_L} = 1125,$$

$$G_{LT} = 0.5\, E_T;\ \ G_{TT} = 0.2E_T;\ \mu_{LT} = \mu_{TT} = 0.25$$

The above material properties indicate that the ratio of transverse to longitudinal Young's modulus is significantly high. This implies that the material is much stiffer along the fibre or longitudinal direction than in the transverse direction. Thermal expansion is highly directional as well, with the transverse coefficient of thermal expansion α_T being 1125 times greater than that in the longitudinal direction α_L. This suggests a pronounced sensitivity to temperature changes perpendicular to fibre alignment. The shear modulus in the longitudinal-transverse plane is defined as $G_{LT} = 0.5\, E_T$, while the shear modulus in the transverse plane is $G_{TT} = 0.2E_T$. This implies different resistance to shear deformation depending on the orientation. The Poisson's ratio for both longitudinal-transverse and transverse-transverse interactions is equal $\mu_{LT} = \mu_{TT} = 0.25$, indicating a moderate degree of lateral contraction when the material is stretched.

3. Results and Discussion

The bilayer (0/90) and three-layer (0/90/0) cross ply simply supported laminated beam structures subjected to thermal line load are considered for flexural analysis. The results of axial displacement, transverse displacement, normal stress, and transverse shear stress are presented in the following normalized form.

$$\overline{u}\left(0, +\frac{h}{2}\right) = \frac{u}{\alpha_L T_1 a}$$

$$\overline{w}\left(\frac{a}{2}, 0\right) = \frac{hw}{\alpha_L T_1 a^2}$$

$$\overline{\sigma}_x\left(\frac{a}{2}, -\frac{h}{2}\right) = \frac{\sigma_x}{\alpha_L T_1 E_T}$$

$$\bar{\tau}_{zx}^{EE}(0,0) = \frac{\tau_{zx}}{\alpha_L T_1 E_T}$$

The normalized axia displacement $\bar{u}$, represents the axial displacement at the top surface of the beam, $\left(z = +{}^{h}/_{2}\right)$, normalized by thermal expansion reference $(\alpha_L T_1 a)$. Normalized transverse displacement $\bar{w}$,

represents the transverse i.e out-of- plane displacement at the mid-span $\left(x = {a}/{2}\right)$. Transverse displacement is normalized by a combination of thermal expansion and geometry $\left(\frac{\alpha_L T_1 a^2}{h}\right)$. Normalized normal stress $\overline{\sigma}_x$ represents the axial stress at the bottom surface $\left(z = -\frac{h}{2}\right)$ at the mid-span. Normal stress is normalized by thermal stress scale $(\alpha_L T_1 E_T)$. The normalized transverse shear stress represents shear stress at the neutral axis $(z = 0)$. Transverse shear stress is normalized by the same thermal stress scale i.e. $(\alpha_L T_1 E_T)$.

3.1. Example:

The two-layer (0/90) and three-layer (0/90/0) simply supported laminated beam structures are considered for the thermal flexural analysis under sinusoidal thermal line load. The trigonometric, parabolic, first-order, and classical theories are applied to evaluate thermal deformation in the beam. Tables 1 and 2 showcase the computed thermal deformation outcome corresponding to aspect ratios of 4, 10, and 100. The ratio of length to thickness of the beam is termed the aspect ratio. The aspect ratio is denoted by "S" in Tables 2, 3, 4, and 5. The axial displacement, transverse displacement, normal stress, and transverse shear stress in the normalized form are shown in Tables 2, 3, 4, and 5 by $\bar{u}$, $\bar{w}$, $\bar{\sigma}_x$, and $\bar{\tau}_{zx}^{EE}$.

The variation of these displacements and stresses across the thickness is shown in Figures 2, 3, 4, 5, 6, and 7. In all these figures, z/h is plotted on the vertical axis, and stresses and displacements are plotted on the horizontal axis.

Table 2. Normalized stresses and displacements in bilayer laminated beam (0/90) under thermal line load.

Model	S	$\overline{u}$	$\overline{w}$	$\overline{\sigma}_x$	$\overline{\tau}_{xz}^{EE}$
		Z= h/2	*Z = 0*	*Z = -h/2*	*Z = 0*
TSDT	4	636.7519	267.0146	13404.74	822.1358
PSDT	4	801.1869	342.9154	10869.56	846.0579
FSDT	4	637.7049	259.3443	13748.33	783.2335
CBT	4	637.7049	259.3443	13748.33	783.2335
TSDT	10	637.5496	255.9322	13692.32	330.3265
PSDT	10	664.3927	272.6293	13398.03	331.8571
FSDT	10	637.7049	259.3443	13748.33	313.2934
CBT	10	637.7049	259.3443	13748.33	313.2934
TSDT	100	637.7034	259.3101	13747.77	33.0610
PSDT	100	637.9726	259.4770	13875.59	33.0625
FSDT	100	637.7049	259.3443	13748.33	33.3293
CBT	100	637.7049	259.3443	13748.33	33.3293

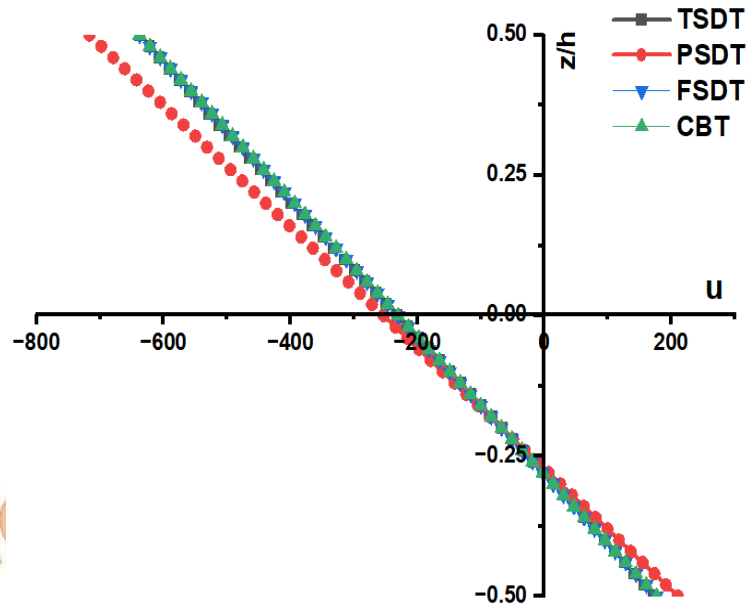

Fig. 2. The distribution of normalized axial displacement ($\bar{u}$) in two layer (0/90) laminated beam under thermal line load for an aspect ratio of 4.

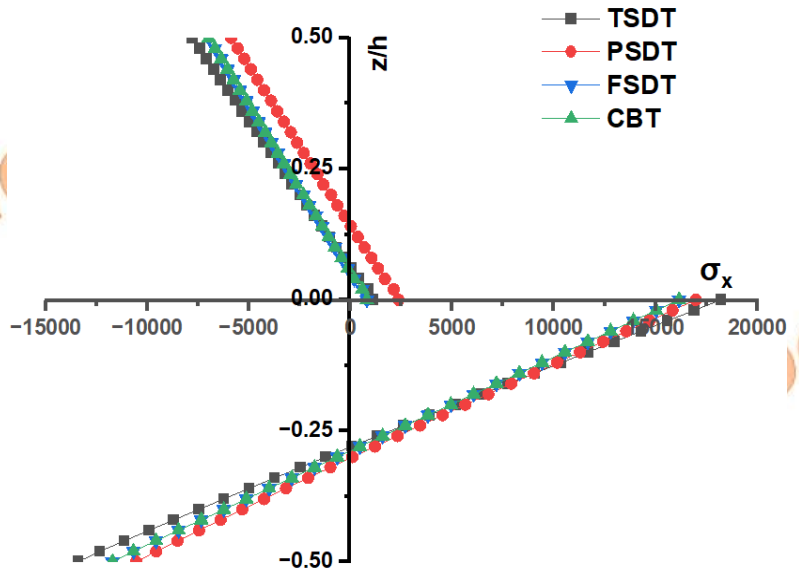

Fig. 3. The distribution of normalized normal stress ($\bar{\sigma}_x$) in two layer (0/90) laminated beam under thermal line load for an aspect ratio of 4.

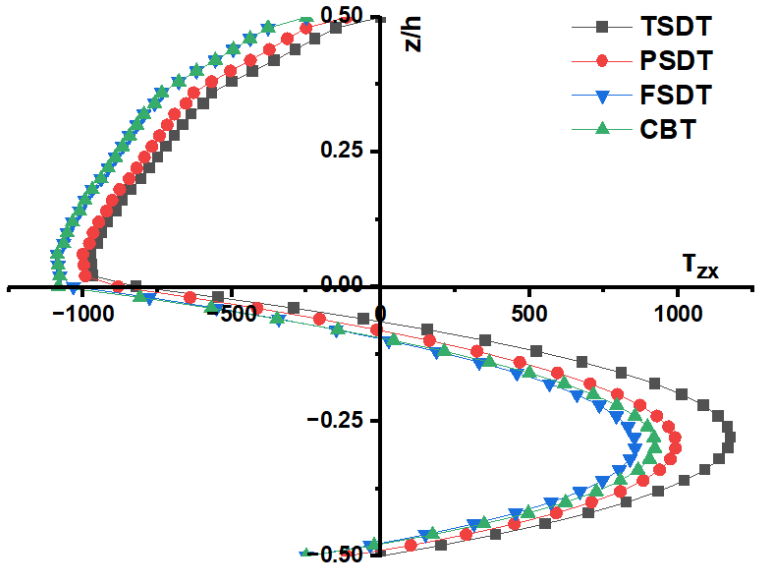

Fig. 4 . The distribution of normalized shear stress ($\bar{\tau}_{zx}^{EE}$) in two layer (0/90) laminated beam under thermal line load for an aspect ratio of 4.

3.1.1 Discussion on Table 2 and Figures 2,3 and 4

1. Axial Displacement ($\bar{u}$) and Transverse Displacement ($\bar{w}$):

Thermal deformations in a two-layer beam structure are presented in Table 2 for aspect ratios 4, 10, and 100. The axial and transverse displacements obtained by parabolic shear deformation theory (PSDT) are higher than the results obtained by trigonometric theory (TSDT) for an aspect ratio of 4. Since axial displacement by PSDT is higher for a thick beam, this suggests that the PSDT theory predicts a more flexible response. Similarly, transverse displacement ($\overline{w}$) evaluated by PSDT for a thick beam is larger than TSDT, indicating that PSDT allows greater transverse deformation. The axial and transverse displacements computed from first-order and classical beam theory have the same values. Further, for aspect ratio 100, these results are identical with each other. The through variation of axial displacement for aspect ratio 4 is shown in Figure 2. The higher values of axial displacements for aspect ratio 4 obtained by PSDT are seen in the figure 2.

For aspect ratio 4, PSDT yields the highest axial displacement (801.1869), which is approximately 25.8% higher than TSDT (636.7519) and 25.6% higher than FSDT and CBT (637.7049). This confirms PSDT's prediction of a more flexible response in a thick beam. As the aspect ratio increases to 10, the axial displacement difference narrows. PSDT result (664.3927) is only 4.2% higher than TSDT (637.5496) and 4.2% higher than FSDT/CBT. When the aspect ratio is 100, all models converge around 637.7, indicating negligible differences and validating that higher aspect ratios reduce the influence of shear deformation.

For a lower aspect ratio 4, PSDT gives the highest transverse displacement (342.91), which is 28.5% higher than TSDT (267.0146) and 32.3% higher than FSDT/CBT (259.34). When the aspect shifts to 10, PSDT (272.62)remains 6.5% higher than TSDT (255.93) and 5.1% higher than FSDT/CBT. For a higher aspect ratio (S =100), all models again converge around 259.3, reinforcing the diminishing effect of shear deformation in beams.

2. Normal Stress ($\bar{\sigma}_x$):

The normal stress obtained by parabolic beam theory is lower than that of the other three theories. This aligns with its higher displacement value of normal stress. This indicated a more compliant behaviour. First order and classical theory's results of normal stress are the highest among the four theories. This implies a stiffer response as compared to other models. The variation of normal stress computed by all four theories is shown in Figure 3.

PSDT consistently predicts lower normal stress across all aspect ratios. For aspect ratio 4, it gives 10869.59, which is 19% lower than TSDT (13404.74) and 20.9% lower than FSDT/CBT (13748.33). At S =10, PSDT (13398.03) is 2.1% lower than TSDT (13692.32) and 2.5% lower than FSDT/CBT. For S = 100, PSDT (13875.59) is slightly 0.9% higher than FSDT/CBT (13748.33), suggesting a reversal in trend due to reduced shear effects.

3. Transverse Shear Stress ($\bar{\tau}_{zx}^{EE}$):

The highest value of transverse shear stress for a thick beam (aspect ratio 4) is obtained by parabolic shear deformation beam theory (PSDT). Whereas trigonometric (TSDT), first-order (FSDT), and classical (CBT) beam theory have slightly lower values of transverse shear stress. This indicates that TSDT, FSDT, and CBT remain stiffer than PSDT. The variation of transverse shear stress across the thickness of the beam is shown in Figure 4. These stresses are continuous at the interface and are computed by equations of equilibrium. The continuity of transverse shear stresses at the interface is important in maintaining the structural integrity of the beam structure.

For aspect ratio 4, PSDT shows the highest shear stress (846.0579), which is 2.9% higher than TSDT (822.1358) and 8% higher than FSDT/CBT (783.2335). For aspect ratio 10, PSDT (331.8571) is marginally 0.5% higher than TSDT (330.3265) and 5.9% higher than FSDT/CBfT (313.2934). For S = 100, all models converge around 33.3, indicating minimal shear stress variation in thin beams.

Table 3. Normalized stresses and displacements in a three-layer (0/90/0) laminated beam subjected to thermal line load.

Model	S	$\bar{u}$	$\bar{w}$	$\bar{\sigma}_x$	$\bar{\tau}_{xz}^{EE}$
		h/2	0	-h/2	0
TSDT	4	5.5434	4.9025	410.7753	87.3386
PSDT	4	5.8530	6.3741	434.6988	80.3841
FSDT	4	5.4531	3.4715	403.2893	86.0016
CBT	4	5.4531	3.4715	403.2893	86.0016
TSDT	10	6.1878	4.5410	406.585	32.7862
PSDT	10	4.8894	4.4149	419.0088	31.0025
FSDT	10	5.4531	3.4715	403.2893	34.4006
CBT	10	5.4531	3.4715	403.2893	34.4006
TSDT	100	5.4757	3.3960	403.5767	3.3253
PSDT	100	5.4511	3.4621	403.1311	3.1672
FSDT	100	5.4531	3.4715	403.2893	3.4400
CBT	100	5.4531	3.4715	403.2893	3.4400

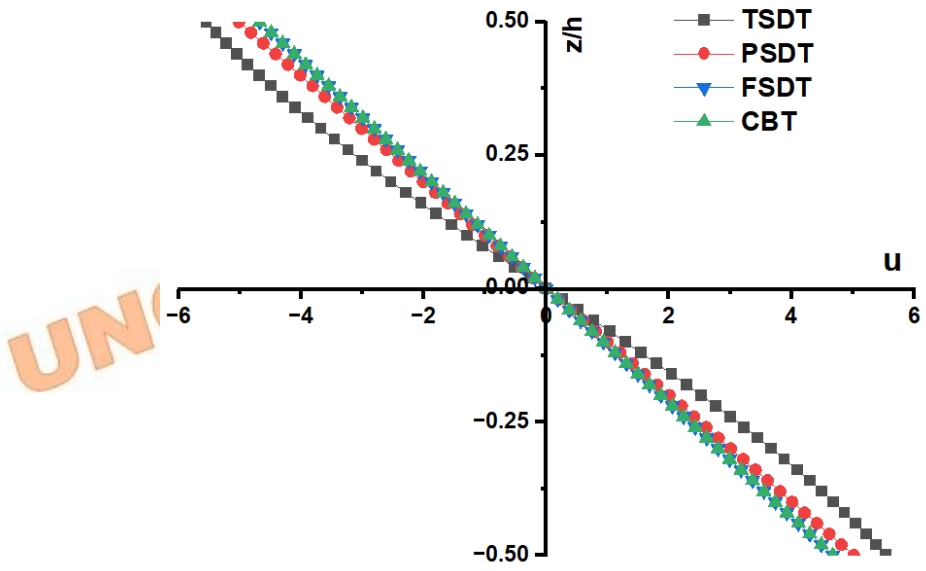

Fig. 5 . The distribution of normalized axial displacement ($\bar{u}$) in (0/90/0) laminated beam structure under thermal line load for an aspect ratio of 4.

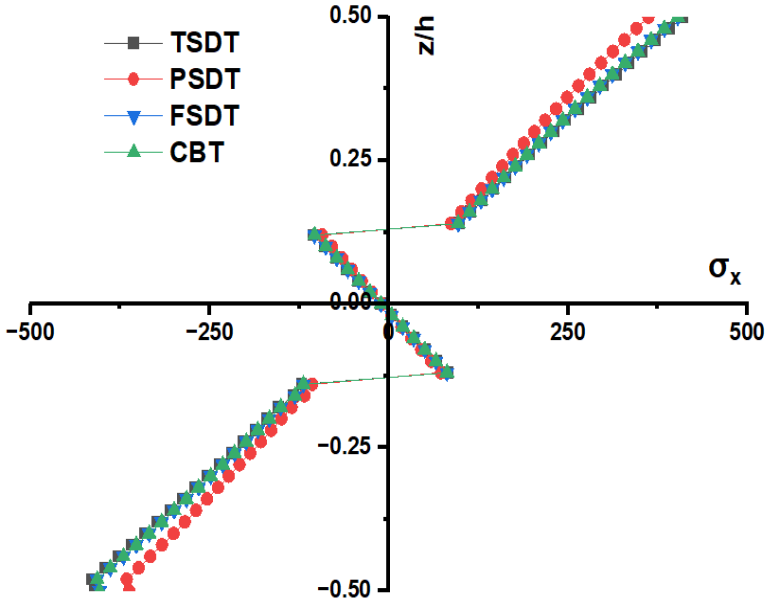

Fig. 6. The distribution of normalized normal stress ($\bar{\sigma}_x$) in three layer (0/90/0) laminated beam under thermal line load for an aspect ratio of 4.

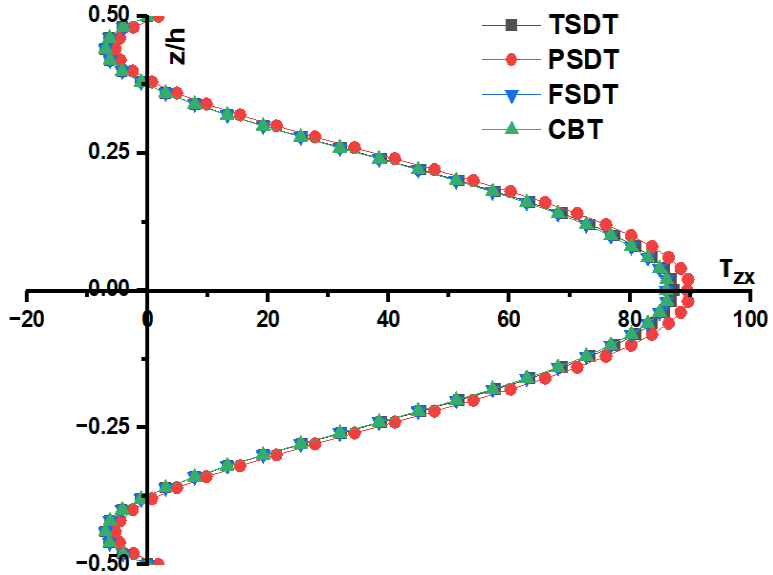

Fig. 7. The distribution of normalized transverse shear stress ($\bar{\tau}_{zx}^{EE}$) in three layer (0/90/0) laminated beam under thermal line load for an aspect ratio of 4.

3.1.2 Discussion on Table 3 and Figures 5,6 and 7

1. Axial ($\bar{u}$) and Transverse Displacements ($\bar{w}$):

Axial displacements obtained by parabolic and trigonometric theories are relatively higher when compared with first-order and classical theories. The transverse displacement obtained by the parabolic (PSDT) model is consistently higher than the other three models for aspect ratio 4. This implies that the PSDT model accounts for higher flexibility in beam response. The results of transverse displacements computed from first-order (FSDT) and classical (CBT) models have identical values due to similar assumptions regarding shear deformation. The variation of axial displacement

along thickness h for an aspect ratio of 4 is shown in Figure 5.

For aspect ratio4, PSDT yields the highest axial displacement (5.85), which is 5.6% higher than TSDT (5.54) and 7.3% higher than FSDT/CBT (5.45). At S = 10, TSDT shows the highest axial displacement (6.18), which is 26.5% higher than PSDT (4.88) and 13.5% higher than FSDT/CBT. For S = 100, all models converge around 5.45 to 5.48, indicating minimal variation and confirming that shear deformation effects diminish in thin beams.

At S = 4, PSDT predicts the highest transverse displacement (6.37), which is 30% higher than TSDT (4.90) and 83.6% higher than FSDT/CBT (3.47). For S =10, PSDT (4.41) is 0.3% lower than TSDT (4.54) but still 27.2% higher than FSDT/CBT. At S = 100, all models show close values around 3.4, with PSDT (3.46) being slightly higher than TSDT (3.39), again confirming convergence in the thin beam.

2. Normal Stresses ($\bar{\sigma}_x$):

The parabolic (PSDT) model predicts higher normal stress for a thick beam (aspect ratio 4). This is followed closely by the trigonometric (TSDT) model, whereas the first-order (FSDT) and classical (CBT) models provide the lower values. The higher value of PSDT indicates a stronger bending response in the beam under thermal loading. Figure 6 illustrates how the axial stress varies throughout the beam's thickness.

For S = 4, PSDT gives the highest stress (434.69), which is 5.8% higher than TSDT (410.77) and 7.8% higher than FSDT/CBT (403.28). At S = 10, PSDT (419.008) remains 3% higher than TSDT (406.585) and 3.9% higher than FSDT/CBT. For S = 100, all models converge near 403.1 to 403.6, indicating reduced sensitivity to model choice at high aspect ratios.

3. Transverse Shear Stress ($\bar{\tau}_{zx}^{EE}$):

The trigonometric shear deformation model (TSDT) predicts higher values of transverse shear stress than the other three models for a thick beam (aspect ratio 4), whereas the parabolic (PSDT) model shows a lower value of shear stress for aspect ratio 4. The thickness dependency is noted when shear stress significantly reduces as the aspect ratio shifts from 4 to 10. The higher values of shear stress by TSDT indicate its accountability for shear deformations. The variation of transverse shear stress across the thickness to beam structure is shown in Figure 7. The equations of equilibrium are used to evaluate these stresses. The continuity of these stresses at the interface and the realistic curve is seen in Figure 7.

At S = 4, TSDT predicts the highest shear stress (87.33), which is 8.6% higher than FSDT/CBT (86.00)and 8.6% higher than PSDT (80.38). For S = 10, TSDT (32.78) is 5.7% higher than FSDT/CBT (34.40), while PSDT (31.00) is 9.9% lower than TSDT. At S = 100, all models converge around 3.3 to 3.4, with PSDT (3.16) being the lowest, confirming the diminishing effect of shear deformation in thin beams.

3.1.3 Validation of Present Model:

The credibility of these higher-order models has been established through a comparative study with benchmark analytical results available in the literature. Laminated composite beams subjected to sinusoidal thermal loading are analyzed, and the obtained dimensionless displacements and stress components are compared with the exact analytical solutions provided by Vidal and Polit [27]. The close correlation between the present predictions and the reference data confirms the precision and robustness of the developed formulation.

Table 4 . Dimensionless deformations and stresses in a two-layer 0/90 composite beam under sinusoidal thermal load

Model	S	$\bar{u}$	$\bar{w}$	$\bar{\sigma}_x$	$\bar{\tau}_{xz}^{EE}$
		h/2	0	*-h/2*	0
TSDT	4	101.3	37.9	2133.4	177.4
PSDT	4	120.2	40.1	1703.9	174.2
SinR*	4	153.3	45.8	1774.5	133.1
Exact*	4	155.3	42.8	1994.7	131.7
TSDT	10	101.4	40.7	2179.2	71.09
PSDT	10	105.5	41.1	2110.5	71.96
SinR*	10	111.8	45.8	2199.8	68.34
Exact*	10	114.1	43.2	2129.0	67.96
TSDT	100	101.4	41.2	2188.0	7.111
PSDT	100	101.5	41.2	2187.3	7.322
SinR*	100	101.6	41.2	2199.8	7.207
Exac*t	100	104.1	43.1	2171.7	7.179

* Exact solution and SinRef-c model [27]

Table 5. Dimensionless thermal deformations and stresses in a three-layer (0/90/0) composite beam under sinusoidal thermal load

Model	S	$\bar{u}$	$\bar{w}$	$\bar{\sigma}_x$	$\bar{\tau}_{xz}^{EE}$
		h/2	0	*-h/2*	0
TSDT	4	0.227	0.609	44.355	14.42
PSDT	4	0.904	2.236	153.67	16.37
SinR*	4	0.260	0.233	4.4627	14.32
Exact*	4	7.469	3.615	281.11	21.41
TSDT	10	0.461	0.722	43.688	9.722
PSDT	10	0.814	1.579	110.17	6.371
SinR*	10	0.734	0.376	32.960	6.585
Exact*	10	5.009	1.893	87.410	7.143

TSDT	10	0.860	0.540	43.210	0.695
PSDT	100	0.866	0.548	42.831	0.673
SinR*	100	0.866	0.550	43.378	0.682
Exact*	100	4.449	2.819	43.310	0.673

* Exact solution and SinRef-c model [27]

The results presented in Tables 4 and 5 show the comparison of displacements and stress components with the exact solution and SinRef model presented by Vidal and Polit [27]. For a smaller aspect rario i.e for a thick beam (S = 4), some discrepancies are observed, primarily due to pronounced transverse shear and normal deformation effects that become significant in thick laminated beams. However, as the beam's aspect ratio increses the computed displacements and stresses from the present higher-order models approach the exact solutions very closely, confirming their consistency and convergence. The results collectively demonstrate that the present formulation is capable of accurately representing thermal behaviour.

4. Coupling Effects

In composited beams, coupling refers to the intricate interactions between various deformation modes, including bending, twisting, and stretching. These interactions arise from the inherent anisotropy of composite materials, where the directional dependence of properties significantly influences the structural response. The accurate prediction of thermal stresses and deformations in composite laminated beams hinges on a thorough understanding of coupling effects. Coupling effects play a crucial role in determining the thermal stress distribution within the beam, which is essential for structural integrity.

Table 2 shows the large axial displacements from 636.7519 to 801.1869, high normal stress ranging from 10,869.56 to 13,800, and significant transverse displacement values from 259.3443 to 342.9154 in the asymmetric laminate (0/90). These values show that thermal loading causes both bending and stretching. Whereas in a symmetric laminated beam (0/90/0), much smaller axial displacement values from 5.4 to 6.2, lower normal stress ranging from 403 to 435, and reduced transverse displacement values from 3.4 to 6.4 are noticed, as in Table 3. This confirms that symmetric stacking suppresses coupling and allows thermal loads to produce bending without significant in-plane effects.

The shear stress is also significantly higher in the asymmetric laminated beam (0/90) at low aspect ratio. As the aspect ratio increases, shear stress drops in both cases but remains consistently lower in symmetric configurations.

These results clearly imply that asymmetric laminates exhibit strong thermal coupling, leading to large displacements and stresses. Whereas a symmetric laminate effectively eliminates coupling, which results in more stable thermal behaviour. Hence, for thermally loaded composite beams, symmetric stacking is preferred to minimize unwanted deformation and stress build-ups.

It is clear that when a composite laminate is asymmetric, like a 0/90 bilayer, it lacks mirror symmetry about its midplane. This asymmetry leads to a non-zero coupling matrix [B] in laminate beam theory, which causes thermal loads to induce bending and stretching, as well as a temperature gradient across the thickness to produce axial displacements and stresses even without mechanical loads.

5. Conclusions

The flexural behaviour of laminated beam structures under thermal line load is studied by using parabolic, trigonometric, first-order, and classical beam theories. The parabolic beam theory allows greater displacement and lower normal stress under thermal line load, indicating its suitability and applicability where flexibility is desired rather than rigidity. The trigonometric beam theory would offer a balanced approach between displacement and stresses, if minimizing shear effects is critical under thermal line load. The shear deformation effects are very dominant in the parabolic beam theory model, due to which transverse displacements and transverse shear stress values are higher than those of the other three theories in the case of a three-layer thick beam. Further, thermal analysis of laminated composite beams using TSDT and PSDT reveals that antisymmetric laminates (0/90) are highly susceptible to thermal coupling, resulting in significant displacements and stress concentrations. On the other hand, symmetric laminates (0/90/0) exhibit greater thermal stability, making them preferable for applications involving sustained thermal exposure. This implies the role of symmetry. Within laminate theory, an antisymmetric configuration (0/90) generates nonzero coupling terms in the [B] matrix, which couple thermal resultants into bending responses. Decomposing the thermal loads shows that the uniform or constant component, , T_0 primarily drives extensional strain, while the gradient component T_1 introduces bending and shear contributions. In an antisymmetric beam T_1 couples strongly into bending, producing significant deflections and localized stress concentration. The symmetric laminated beam

(0/90/0), by contrast nullify [B] matrix, thereby suppressing thermal coupling and confining the thermal resultants to extension alone. This structural symmetry explains their superior thermal stability under sustained exposure. The distinction between parabolic shear deformation theory (PSDT) and trigonometric shear deformation theory (TSDT) becomes particularly relevant for thick beams. The PSDT incorporates transverse normal strain effects and assumes a parabolic shear distribution, which enhances flexibility but also magnifies shear stresses. Another higher-order trigonometric shear deformation theory (TSDT) with its trigonometric distribution better captures the decay of shear stresses through the thickness of the beam, thereby reducing displacement predictions while maintaining accuracy in stress evaluation. These differences highlight that PSDT's apparent flexibility arises from its treatment of transverse strain fields rather than a simple relaxation of stiffness. Therefore, the applicability of refined theories relative to first-order (FSDT) and Classical (CBT) beam theory depends on the aspect ratio. For larger aspect ratio i. e. for 100, refined models converge with FSDT/CBT predictions, while for smaller aspect ratio i. e. for thick beam (S = 4), deviations become significant. Hence, refined models are essential to capture shear and thermal coupling effects accurately in thick and thin beams.

These findings emphasize the importance of laminate symmetry in structural design and thermal management, offering valuable guidance for engineers and researchers in composite material applications. A possible extension of this work is to optimize the thermal response of composite laminated beams under thermal loadings.

Acknowledgments

The authors acknowledge the Symbiosis Institute of Technology, Pune, for their encouragement and continuous support.

Funding Statement

This research did not receive any specific grant from funding agencies in the public, commercial, or not-for-profit sectors.

Conflicts of Interest

The authors declare that there is no conflict of interest regarding the publication of this article.

References

[1] Chen, D., Cheng, S. and Gerhardt, T. D. 1982. Thermal stresses in laminated beams. *Journal of Thermal Stresses*, 5, pp. 67–84.

[2] Timoshenko, S. P. , 1921. On the correction for shear of the differential equation for transverse vibrations of prismatic bars. *Phil Mag Ser*, 41, pp. 744–764.

[3] Miglani, J., Devarajan, B. and Kapania, R. K. 2018. Thermal buckling analysis of periodically supported composite beams using Isogeometric analysis. *AIAA/ASCE/AHS/ASC Structures, Structural Dynamics, and Materials Conference*, p. 122. 4

[4] Chen, W., Li, L. and Xu, M., 2011. A modified couple stress model for bending analysis of composite laminated beams with first order shear deformation. *Composite Structures*, 93, pp. 2723–2732.

[5] Kapuria, S., Dube, G. P., Dumir, P. C. and Sengupta, S., 1997. Levy-type piezothermoelastic solution for hybrid plate by using first-order shear deformation theory. *Composites Part B: Engineering*, 28, pp. 535–546.

[6] Touratier, M., 1991. An efficient standard plate theory. *International Journal of Engineering Science* ,29, Issue 8, pp. 901-916 https://doi.org/10.1016/0020-7225(91)90165-Y

[7] Ali, J. S. M., Bhaskar, K., Varadan, T. K., 1999. A new theory for accurate thermal /mechanical flexural analysis of symmetric laminated plates, *Composite Structures,* 45 (3), pp227-232.

[8] Robaldo, A. and Carrera, E., 2007. Mixed finite elements for thermoelastic analysis of multilayered anisotropic plates. *Journal of Thermal Stresses*, 30, pp. 165–194.

[9] Kant, T. and Gupta, A., 1988. A finite element model for a higher-order shear-deformable beam theory. *Journal of sound and vibration*, 125, pp. 193–202.

[10] Khedir, A., A. and Reddy, J.,N., 1994. Free vibration of cross–ply laminated beams with arbitrary boundary conditions. *International Journal of Engineering Science*, vol. 32(12), pp. 1971–1980. https://doi.org/10.1016/0020-7225(94)90093-0

[11] Babu, C. S. and Kant, T., 2000. Refined

higher-order finite element models for thermal buckling of laminated composite and sandwich plates. *Journal of thermal stresses*, vol.23, 111–130.

[12] Ghugal, Y. M. and Shimpi, R. P., 2001. A review of refined shear deformation theories for isotropic and anisotropic laminated beams. *Journal of Reinforced Plastics And Composites,* 20(3), pp. 255–272. https://doi.org/10.1177/073168401772678283

[13] Arya, H., Shimpi, R. P. and Naik, N. K., 2002. A zigzag model for laminated composite beams. *Composite structures*, vol. 56, pp 21–24.

[14] Carrera, E., 2005. Transverse normal strain effects on thermal stress analysis of homogeneous and layered plates. *AIAA Journal*, 43(10), pp. 2232-2242.

[15] Carrera, E., Giunta, G. and Petrolo, M., 2011. Beam Structures: Classical and Advanced Theories, John Wiley & Sons Ltd U.K.

[16] Aydogdu, M., 2007. Thermal buckling analysis of cross-ply laminated composite beams with general boundary conditions. *Composites Science and Technology*, 67, pp. 1096–1104.

[17] Ghugal, Y. M. and Sharma, R., 2009. A hyperbolic shear deformation theory for flexure and vibration of thick isotropic beams, *International Journal of Computational Methods,* 6(4) pp. 585–604. https://doi.org/10.1142/S0219876209002017

[18] Vidal P. and Polit O., 2006. A thermomechanical finite element for the analysis of rectangular laminated beams, *Finite Elements in Analysis and Design*, 42 (10), pp. 868-883.

[19] Sayyad A.S., 2011. Comparison of various refined beam theories for the bending and free vibration analysis of thick beams. *Appl Comput Mech*, 5, pp. 217–230.

[20] Sayyad A. S. and Ghugal Y. M., 2011. Effect of transverse shear and transverse normal strain on bending analysis of cross-ply laminated beam. *International Journal of Applied Mathematics and Mechanics*. **7** (12): pp. 85-118

[21] Chang, X. P., Liu, J. and Ren, J. H., 2012. Thermal Post-Buckling of Heated Cross-Ply Laminated Composite Beams. *Applied Mechanics and Materials*, 105, pp. 2321–2324.

[22] Ghugal, Y. M. and Dahake, A. G., 2012. Flexural analysis of deep beam subjected to parabolic load using refined shear deformation theory, *Applied and Computational Mechanics*, 6.pp.163–172.

[23] Li, Z.-M. and Qiao, P., 2015. Thermal postbuckling analysis of anisotropic laminated beams with different boundary conditions resting on two-parameter elastic foundations. *European Journal of Mechanics-A/Solids*, 54, pp. 30–43.

[24] Mohammadabadi, M., Daneshmehr, A. R., and Homayounfard, M., 2015. Size-dependent thermal buckling analysis of micro composite laminated beams using modified couple stress theory. *International Journal of Engineering Science*, 92, pp. 47–62.

[25] Sayyad, A. S. and Ghugal, Y. M., 2017. Bending, buckling and free vibration of laminated composite and sandwich beams: A critical review of literature. *Composite Structure*, 171, pp. 486–504 https://doi.org/10.1016/j.compstruct.2017.03.053

[26] Bhaskar, K., Varadan, T. K., Ali, J. S. M., 1996. Thermoelastic Solutions for Orthotropic and Anisotropic Composite Laminates. *Composite part B: Engineering* 27-B, pp. 415-420.

[27] Vidal P, and Polit O., 2009. A Refined Sine-Based Finite Element with Transverse Normal Deformation for the Analysis of Laminated Beams under Thermomechanical Loads. *Journal of Mechanics and Material Structures*. **4**, pp 1127–1155.

[28] Kenanda, M., Hammadi, F., Zouari, W., Belabed, Z., Ayad, R., 2025. Thermo-mecchanical free vibration analysis of porus FGM plates resting on Kerr'sfoundation

using a new logarithmic-hyperbolic shear deformation theory. *Archive of Applied Mechanics*. 95, https://doi.org/10.1007/s00419-025-02779-7

[29] Taibi, N., Belabed, Z., Boucham, B., Benguediab, M., Tounsi, A., Khedher, K. M., Salem, M. A., 2024. On the thermomechanical behaviour of laminated composite plates using different micromechanical-based models for coefficients for thermal expansions (CTE). *Journal of Applied and Computational Mechanics.* 10, pp. 224-244. https://doi.org/10.22055/jacm.2023.44257.4191

[30] Kenanda, M. A., Hammadi, F., Bahai, H., Belabed, Z., 2026. A new efficient nonlocal hyperbolic HSDT for mechanical vibration of porus FGM plates/nanoplates using Navier's method and artificial neutral network prediction. *International Journal of Solids and Structures,* 325, 113719. https://doi.org/10.1016/j.ijsolstr.2025.113719.

[31] Reddy, J. N., 1984. A simple higher-order theory for laminated composite plates, *Journal of Applied Mechanics,* 51 (4), pp. 745-752.

[32] Radojkovic, M., Stojanovic, B., Milojevic, S., Maric, D., Savic, S., Skulic, A., Krstic, B., 2023. Square openings as sources of stress concentration in parts of machines and devices, *Technical Gazette,* 30 (2), pp. 474-480. https://doi.org/10.17559/TV-20220603080026.

[33] Marinkovic, D., Dezso, G., Milojevic, S., 2024. Application of machine learning during maintenance and exploitation of electric vehicles. *Advanced Engineering Letters,* 3(3), pp. 132-140. https://doi.org/10.46793/adeletters.2024.3.3.5

[34] Gajevic, S., Markovic, A., Milojevic, S., Asonja, A., Ivanovic, L., Stojanovic, B., 2024. Multi-objective optimization of tribological characteristics for aluminium composite using taguchi Grey and TOPSIS Approaches, *Lubricants.* 12, 171. https://doi.org/10.3390/lubricants12050171